Laser-assisted methods for nanofabrication

Andrei V. Kabashin, Michel Meunier

Laser Processing Laboratory, Department of Engineering Physics, Ecole Polytechnique de Montreal, Case Postale 6079, Succ. Centre-ville, Montreal, Quebec, Canada, H3C 3A7

ABSTRACT

An overview of laser-assisted nanofabrication methods, which has been developed in the Laser Processing Laboratory, is presented. All methods imply the laser-related ablation of material from a solid target and the production of nanoparticles or nanostructures. We consider the nanofabrication process in both the gaseous and in the liquid ambience under different parameters of laser radiation. A particular attention is given on the absence or presence of the plasma-related absorption of the laser radiation, which make possible different nanofabrication regimes. The methods lead to a production of nanomaterials, which are of importance for photonics and biosensing applications.

Keywords: laser-assisted nanofabrication, nanoparticles, nanostructures, laser ablation

I. INTRODUCTION

Some properties of laser radiation make it very interesting for tasks of nanofabrication. The radiation can be efficiently transmitted through solid, gaseous and liquid media and its energy can be easily concentrated in almost any point by the use of focusing optical elements. When focused on a solid target, intense laser radiation can cause the melting and then the ablation of the material from the target[1], leading to the ejection of atoms and nanoclusters[2-4]. The further nanocluster growth is determined by both laser parameters (wavelength, pulse length, fluence) and properties of the ambient medium. Here are the following possibilities:

1. A pure laser ablation when the plasma is transparent to laser radiation. In this case, the radiation ablates the target and thus produces nanoclusters, which then cool down through their interaction with ambient environment (Fig. 1a). If the nanoclusters are produced in a gaseous environment, they can then be deposited on a substrate forming a thin nanostructured film. As another possibility, the ablation in liquids leads to the release of material to the liquid and the formation of colloidal nanoparticle solution.

2. The production of laser-assisted breakdown plasma, which strongly absorbs the incoming radiation and reduces the radiation-related ablation efficiency[5] (Fig. 1b). In general, conditions for the breakdown plasma production exist in both gaseous and liquid environment. In particular, we recently showed[6-11] that this hot plasma can be used to heat the material of a semiconductor target and thus transform its properties.
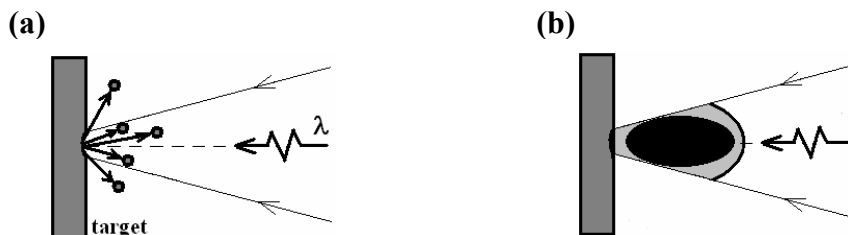
(a)　　　　　　　　　　　　　**(b)**

Fig. 1 (a) Pure laser ablation regime; (b) Optical breakdown regime.

Three different methods have been recently developed in the Laser Processing Laboratory that use both the laser ablation and the optical breakdown regimes. These methods are the pulsed UV laser deposition of nanostructured Si-

based films in a residual gas[12-16], CO_2 laser-produced optical breakdown processing of semiconductors[6-11], and femtosecond laser ablation of metals in aqueous solutions[17-19]. This paper focuses on the overview of these methods.

II. LASER ABLATION OF SILICON IN RESIDUAL GAS AND DEPOSITION OF SI-BASED NANOSTRUCTURED FILMS

The interest to nanostructured semiconductors is primarily due to their particular photoluminescence (PL) properties. Bulk Silicon and Germanium are group IV semiconductors, which have indirect and small band gaps (1.1 eV for Si and 0.6 eV for Ge) and do not emit visible light. However, these materials become photoluminescent if one performs their nanostructuring or the size reduction down to the nanoscale range. The nanostructuring can be produced either by a wet anodical (chemical) etching (see, e.g., Refs. 20, 21) or by the deposition of a thin nanostructured film (see, e.g., Refs. 22-25). Although the origin of visible PL is still disputable (both the quantum confinement[20] and oxygen-related defects[21,23] are now considered as possible PL mechanisms), these nanomaterials are of importance for photonics and biosensing applications.

Nanostructured Si-based films can be formed by the laser ablation from a silicon target in a residual gas, followed by the deposition of material on a substrate[26-30]. The growth of nanoclusters is usually controlled in the gaseous phase by the presence of a neutral residual gas such as He, which cools them down to produce 1-10 nm nanoparticles on the substrate[27-30]. However, reported PL properties of the nanostructured films prepared by the laser ablation or other deposition techniques were rather different with the presence (see, e.g., Refs. 22, 24) or absence (see, e.g., Refs. 21, 23, 27-29) of the size dependence of the PL spectra, one of main characteristics of the quantum confinement mechanism[20].

In our experiments, we mainly studied possibilities for the control of properties of the deposited films by a variation of radiation parameters[12-16]. Radiation of a pulsed KrF laser (λ = 248 nm, pulse length 15 ns FWHM, repetition rate 30 Hz) was used to ablate the material from a rotating Si target ((1-0-0), N-type, resistance 10 Ohm·cm). The radiation was focused on a focal spot 2x1 mm^2 on the target at the incident angle of 45° giving the radiation intensity of $5 \cdot 10^8$ W/cm^2. The substrates, identical to the target, were placed on a rotating substrate holder at 2 cm from the target. The experimental chamber was pumped down to P = $2 \cdot 10^{-7}$ Torr before filling with helium (purity 99.99995%) for a deposition at a constant pressure P ranging between 0.05 Torr and 10 Torr. The film thickness after several thousands laser shots was 100 – 700 nm.

First, our studies confirmed conclusions of previous works[26-30] that the size of nanoparticles produced by laser ablation can be reduced down to few nanometers when a residual neutral gas (helium) is present during the experiment. A typical Atomic Force Microscope (AFM) image of several isolated laser-ablated particles, deposited on highly oriented pyrolitic graphite (HOPG), is shown in Fig. 2a, while Fig. 2b presents two profile analysis of the image. One can see that the height of the particles was about 2-4 nm, while their recorded lateral dimensions were about 20-30 nm. It is known that real size of nanoobjects is truly presented only by the height measurements, while their lateral dimensions are usually enlarged due to the tip-object convolution effect. Therefore, we may conclude that the real size of the smallest ablated particles was about 2-3 nm that is in agreement with previous studies of laser-ablated Si-based films. One can also see from Fig. 2c that the particles size somewhat decreased with the decrease of helium pressure.
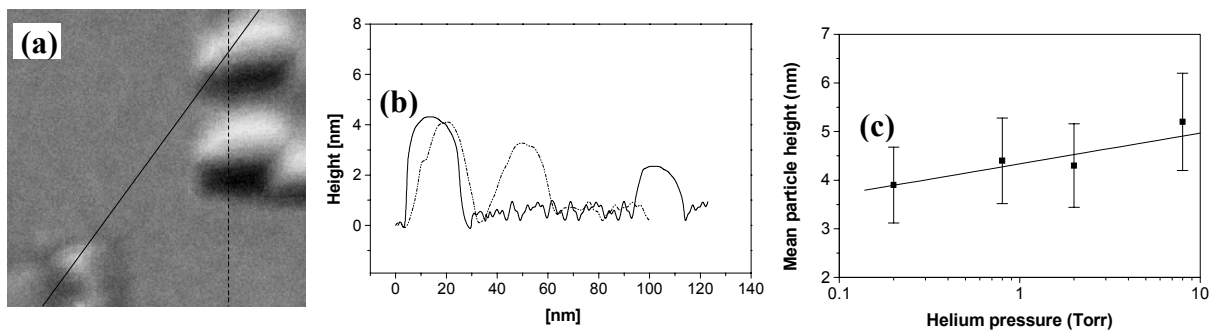

Fig. 2 (a) AFM image of isolated laser-ablated particles on graphite (HOPG) substrate; (b) Profile analysis of the AFM image over the solid and dashed lines; (c) Mean particle height from AFM images as a function of helium pressure during the deposition.

However, we found that the resulting microstructure of the films formed on the substrate depends not only on the size of the ablated particles, but also on conditions of their condensation on the substrate. That is, if particles crystallized in the gaseous phase, they arrived on the substrate in the form of a powder. This situation occurred when the pressure of He was too high or the target-substrate distance was relatively large that caused significant cooling of the nanoclusters before reaching the substrate. Basically, the films suffered microfragmentation with the increase of the helium pressure, as one can see from Scanning Electron Microscopy (SEM) images of the laser-ablated films (Fig. 2a-d). While the deposition under 1 Torr resulted only in some germs of roughness, the experiment under 2 Torr provided a developed porous structure with pore size of about 50-100 nm. Further pressure increase up to 4 Torr led to a formation of web-like aggregations of particles. Note that at P < 1 Torr the roughness details were too small to be detected by our SEM system. The porosity of the laser-ablated films was estimated by using methods of Specular X-ray Reflectivity[31] and the results of these estimations, shown in Fig. 3e, suggested that the porosity of the films gradually increased with the increase of the helium pressure and exceeded 90% for the films deposited at relatively high pressures.
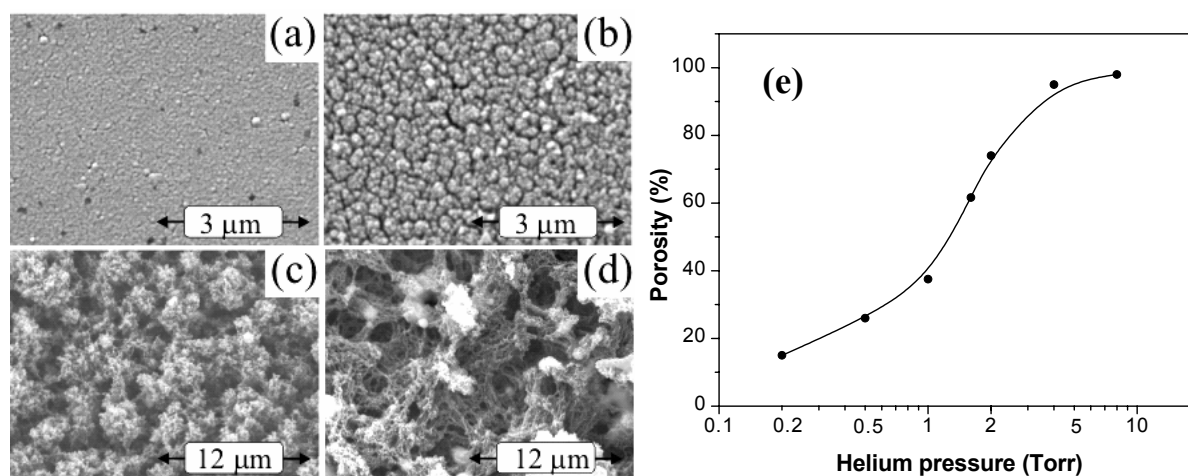

Fig. 3 SEM images of Si-based films fabricated under different pressures of ambient helium: 1 Torr (a), 2 Torr (b), 4 Torr (c), 8 Torr (d). (e) Porosity of the films estimated from SXRR curves as a function of helium pressure during the deposition.

PL properties of the laser-ablated films were also quite different for the films deposited at different helium pressures. Low-porous films deposited at reduced pressures P < 1.5 Torr exhibited relatively weak PL with peak energy strongly depending on the pressure. In particular, the pressure decrease from 1.5 to 0.15 Torr in different depositions caused a blue shift of the peak from 1.6 eV to 2.15 eV to, as shown in Fig. 4a. However, films with an enhanced porosity deposited at P > 1.5 Torr provided only spectra with fixed peaks. The first band (1.6-1.7 eV) was independent of the pressure and could be seen just after the fabrication process, while the prolonged oxidation of the films led to a significant increase of the integral intensity of such PL signals, as shown in Fig. 4b. In addition, an additional band (2.2-2.3 eV) could appear under the oxidation of samples in humid air or the thermal annealing of all as-deposited films, or an addition of pure oxygen into the vacuum system during the deposition process (Fig. 4b). Basically, PL properties of low porous films (porosity < 40%) were almost unchangeable under the prolonged natural oxidation, while the integral PL intensity from highly porous films significantly increased with the prolonged oxidation (Fig.4c).

It was concluded that this was the porosity difference that caused the dramatic distinction of long-term PL properties. Dense and self-coagulated structures of the films fabricated under P < 1 Torr minimized the impact of ambient atmosphere on the film properties. For these films, mechanisms related to core silicon crystals became predominant, although the upper surface oxide could also play a certain role in a formation of PL centers. In particular, the blue shift of the spectra under the decrease of helium residual pressure (Fig. 4a) was accompanied by a certain decrease of the nanocrystal size (Fig. 2c), suggesting the involvement of the quantum confinement mechanism[20]. On the other hand, the porosity enhanced the surface area, which was subjected to surface chemistry modifications due to interactions of nanocrystallites with oxygen and other elements or impurities in ambient air. This could drastically enhance the role of

oxidation in the formation of PL centers and lead to a domination of oxygen-related PL mechanisms connected either to defects in the SiO$_2$ structure (usually, this mechanism provides PL peaks around 2-2.4 eV)[21] or to the interfacial layer (1.65 eV)[23]. In our study, laser-ablated films with porosities higher that 40% exhibited 1.6-1.7 eV and 2.1-2.2 bands (Fig. 4b), whose generation was consistent with defect-related mechanisms.
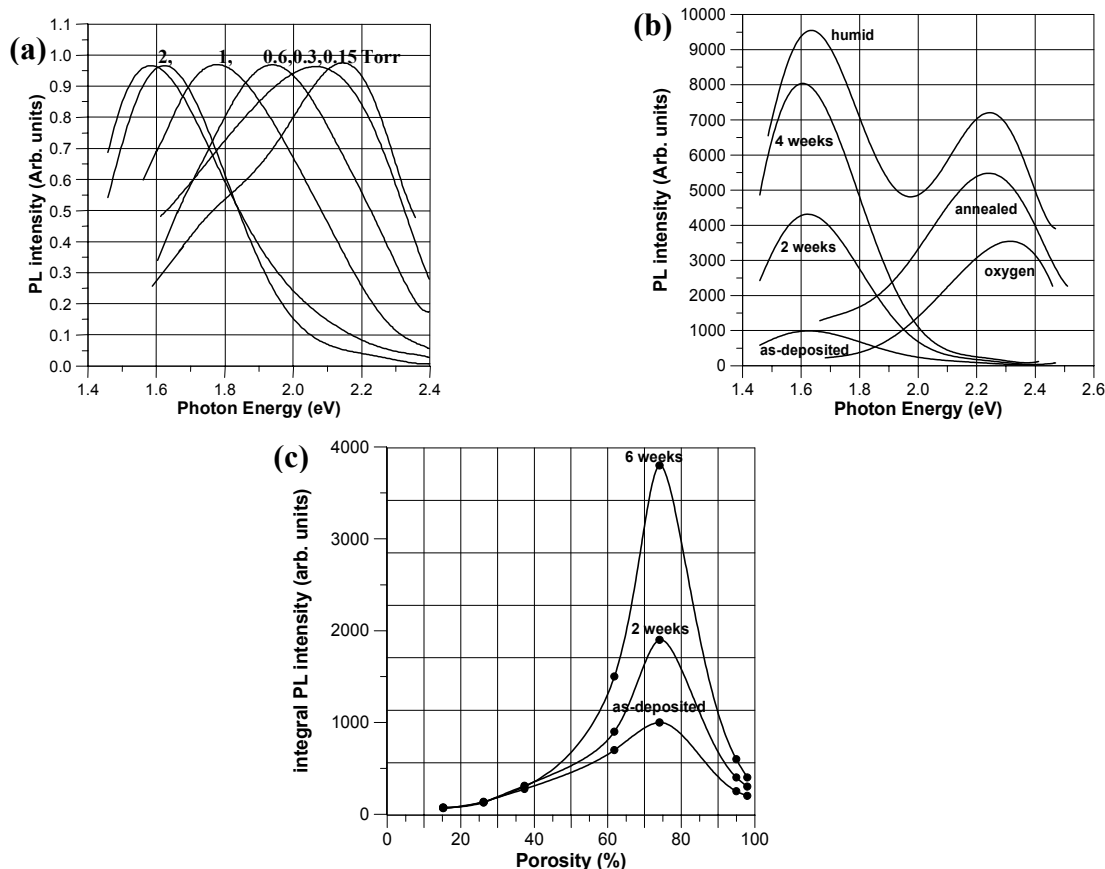

Fig. 4 (a) Photoluminescence spectra of the laser-ablated Si-based films deposited at different helium pressures; (b) PL spectra of the films prepared at after 4 hours, 2 weeks, 4 weeks of the film exposition to dry air; after 8 weeks of the exposition in humid air; and after the thermal annealing. (c) Integral intensity of PL signals as a function of film porosity under a prolonged storage of the films in dry ambient air.

   Thus, a technique of laser ablation from a Si target in a residual helium gas has been used to produce Si nanoclusters and deposit them on a substrate to form Si-based nanostructured films. In addition, our works[12-16] have unambiguously showed that not only the mean particle size, but also the film microstructure (porosity) is strongly affected by a variation of deposition conditions. We also found that the film porosity can control the impact of oxidation and thus determine PL properties (quantum confinement or oxygen-related mechanisms). Finally, our results suggest that the reported discrepancy of experimental results related to the presence[22,24] or absence[21,23,27-29] of the size dependence for the PL peak position were probably related to different film microstructures obtained in different studies. Relatively porous films could provide better conditions for oxidation-related mechanisms, while low porous films contributed to preferential contribution of other mechanisms, e.g., the quantum confinement one.

III. OPTICAL BREAKDOWN PROCESSING OF SEMICONDUCTORS

In the proposed diagram of Fig. 1, the optical breakdown phenomenon corresponds to the case of highly absorbent plasma (b). In general, the gas breakdown can be produced even in the absence of the target by simply focusing IR

radiation in a gas at a relatively high pressure. The presence of a target decreases the breakdown threshold by 2-3 orders of magnitude and then hot, highly absorbent plasma is formed in the ambient gas[5]. Our idea, as introduced in Refs. 6-11, was the use of the breakdown plasma to treat semiconductors and thus produce their local nanostructuring. The proposed method is somewhat similar to the electric spark processing, in which a unipolar electric discharge is initiated between two electrodes to treat one of them[32-35]. However, the laser-assisted method does not use high voltages, which is important for some specific applications such as the processing of an assembled semiconductor device or microchip, and is expected to shorten the processing time.

We produced the optical breakdown by focusing the radiation from a pulsed CO_2 laser (wavelength 10.6 µm, pulse energy 1 J, pulse length 1 µs FWHM, repetition rate 3 Hz) on a Si or Ge target in atmospheric pressure gases. Standard Si and Ge wafers (resistance 0.01- 10 Ohm·cm) with dimensions of about 1×1 cm^2 were used as targets. The tests were performed in different ambient gases, such as O_2, air, N_2, Ar, He, having the ionization potentials of 13.6 eV, 14.3 eV, 14.5 eV, 15.8 eV, and 24.6 eV, respectively. For comparison, we also carried out conventional ablation tests with the use of KrF laser radiation (248 nm, 30 ns FWHM, 3 Hz) in similar experimental conditions. Since 248 nm is hardly absorbed by the plasma, the ablation of material should take place in the breakdown-free regime.

The experiments showed that the layers produced by the optical breakdown processing and UV laser ablation were quite different. For the optical breakdown, the crater under the irradiation spot was almost absent and the deposition of material outside the spot was weak or absent. The layers themselves presented highly porous material with holes between 30 and 150 nm, as shown in Fig. 5a. Similar porous structures were observed under the breakdown treatment of the semiconductors in all other gases, except oxygen. For O_2, with the lowest ionization potential, the porosity appeared to be absent, while the treated surface contained clearly visible traces of a molten material (Fig. 5b). In contrast, the UV ablation of Si and Ge led to a formation of craters under the spot and a considerable deposition of material around the crater, while the crater bottom contained microscale spikes (Fig. 5c). The different properties of layers produced by UV and IR laser irradiation of silicon were apparently related to different conditions and parameters of the plasma-assisted processes. Since UV radiation is well absorbed by the semiconductor target, it leads to an efficient ablation of the material of the target and to the plasma production. However, the plasma itself does not absorb strongly the UV radiation power and remains almost transparent to the incoming radiation. Therefore, the ablation of material remains efficient during the whole laser pulse and the ablated material rapidly cools down due to collisions with dense air elements, yielding to its deposition on the surrounding target surface. The formation of microspikes is probably explained by a difference of light absorption efficiencies in different points on the target. On the other hand, the interaction of the CO_2 laser radiation with matter is characterized by a fast transition from a target-related to a plasma-related radiation absorption[5]. The target generates initial electrons to ignite the gas discharge, which then develops in the cold gas toward the focusing lens, absorbing main IR radiation power and, as a consequence, getting heated up to high temperatures of more than 10^4 K. The radiation causes a localized melting and even flash evaporation of the target material. This process probably takes place only in some casual points, which causes the appearance of pores on the target surface. The laser-ablated material and the upper target layer are then heated by the hot breakdown plasma during milliseconds, leading to additional phase transformations and the initiation of chemical reactions in the plasma. The plasma-related modification of material is especially visible in the case of O_2 with the lowest ionization potential. Indeed, for O_2 the treated surface was molten, with the absence of pores, suggesting that the temperature of the breakdown plasma was sufficiently high to melt the material of the upper target layer.
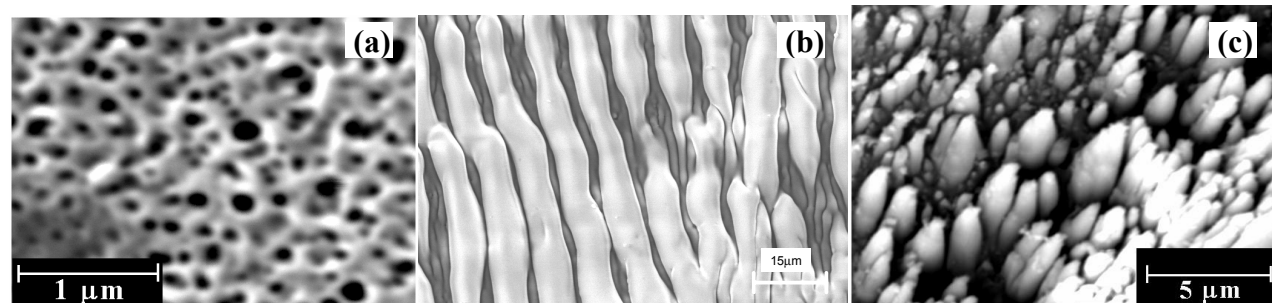

Fig. 5 SEM photomicrographs of Si after several breakdown initiations in air (a), O_2 (b) and after UV laser ablation in air (c).

The structural properties of the layers and their composition were studied by X-ray diffraction (XRD), transmission electron microscopy (TEM) X-ray photoelectron spectroscopy (XPS), and photoacoustic FTIR. We found that the layers were nanostructured and mainly composed of Si (Ge) nanocrystals (2-10 nm) embedded into SiO_2 (GeO_2) matrix. The prolonged aging of samples in ambient air led to the increase of oxygen content in the film composition.

The layers formed by the optical breakdown exhibited strong visible PL that could be seen by naked eyes. PL peak was around 2 eV (Fig. 6a) and 2.2 eV (Fig. 6b) for Si and Ge, respectively, while a prolonged exposition of the layers to ambient air led to a slight blue shift of PL peak positions by 0.2 eV. The intensity of PL emission depended on the optical breakdown plasma intensity, which was finally determined by the ionization potential of the ambient gas. The strongest PL intensity was observed for layers prepared in O_2, followed by those prepared in air, N_2 and Ar and He. In contrast, the surface ablated by the excimer laser yield to much weaker PL signals (integral PL intensity was weaker by an order of magnitude) with the peak position between 2.0 and 2.3 eV (Fig. 6c). These signals were not uniform over the sample and differed drastically from point to point, as shown in Fig. 3(b). Furthermore, it was difficult to draw any dependence of PL peak position on a number of laser shots.
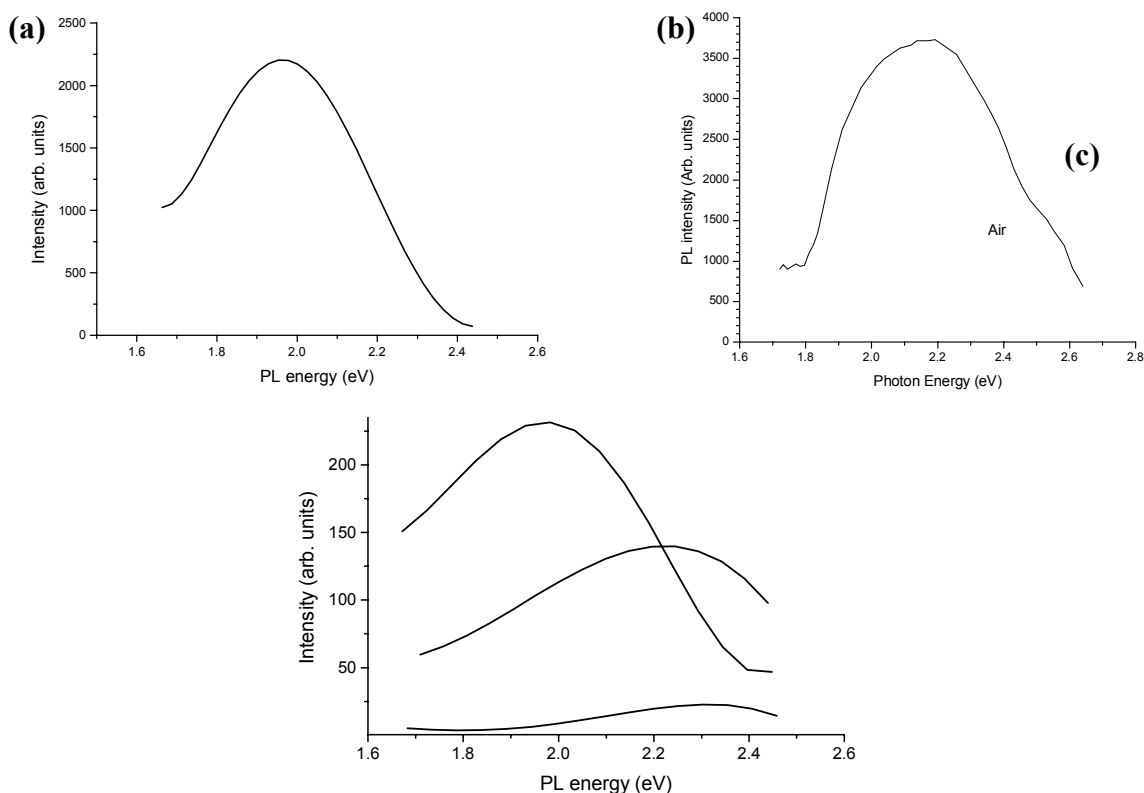

Fig. 6 Typical PL spectra from Si (a) and Ge (b) targets after their breakdown processing by 500 laser shots. (c) Typical PL spectra from different regions of the target surface after 500 shots of the excimer laser.

The mechanism of visible PL emission is still not well understood. Some experimental facts such as the blue shift of PL during the prolonged oxidation of layers suggest that PL origin can be related to the quantum confinement mechanism[20]. Indeed, the mentioned increase of the oxygen content during the aging can be accompanied by the decrease of the Si nanocrystal size in the SiO_2 matrix that should lead to the blue shift of the PL peak according to the quantum confinement model, as it was observed in many studies (see, e.g., Refs. 22, 24). However, other mechanisms could also be responsible for the observed PL signals. In particular, the observed signals could be related to defects in

the SiO_2 matrix, which also exhibit PL in 2.0-2.4 range[36]. In this case, the blue PL shift on aging in air can be related to larger stress introduced by the prolonged oxidation.

In summary, we showed in these works[6-11] that highly absorbent plasma of the optical gas breakdown can be used to locally treat semiconductors, transforming their surface to a porous nanostructured material. Exhibiting strong PL emission in the visible, the produced porous nanostructured layers are of importance for both optoelectronics and biosensing applications.

IV. LASER ABLATION FROM A SOLID TARGET IN AQUEOUS SOLUTIONS

The third nanofabrication approach is related to the laser ablation in a liquid environment to produce colloidal metal (Au, Ag, Pt, Cu) and semiconductor (Si) nanoparticles. These nanoparticles are of interest for biomolecular recognition tasks, in which they can be used, after an appropriate surface modification and linking with biological objects, as markers of biological objects. In this case, the presence of these objects can be screened by a change of optical characteristics of the nanoparticles. For semiconductors, the most suitable sensing parameter is PL signals. For metals, this could be nanoparticles-related extinction (absorption + scattering) spectra, since these spectra strongly depend on both the nanoparticle size and a mean distance between them due to the generation of Mie resonances[37] and to quantum size effects (below 3 nm)[38]. For example, 3-30 nm gold nanoparticles are known to provide plasmon-related absorption peak around 520 nm and transmit all longer wavelengths, giving rise to a red coloration of gold nanoparticle solutions.

Colloidal metal or semiconductor nanoparticles can be fabricated by a chemical method, in which a diluted metal salt is reduced in an aqueous solution with a reducing reagent[39]. However, the particles are formed in dirty environment with different impurities that complicate a further stabilization and functionalization of the gold surface for biological immobilizations. Although chemically prepared particles can be used for some biosensing tasks, alternative methods of the nanofabrication in a clean, well-controlled environment are still needed. In contrast to many other material ablation techniques, laser ablation gives some unique possibilities for the nanomanipulation in liquids. The radiation energy can be effectively transmitted through a liquid environment and concentrated on a solid target to achieve the ablation of material directly in liquids and thus produce colloidal nanoparticles. Many authors used nanosecond lasers to ablate Au and Ag target in aqueous environment[40-49]. However, the size distribution of the nanoparticles in liquids tends to be broadened since the aggregation process of hot ablated atoms after the ablation process cannot be easily overcome. Several attempts have been made for the size control and the most efficient results were obtained by the use of aqueous solutions of surfactants such as sodium dodecyl sulfate (SDS), which covered the surface of nanoparticles and thus prevented them from the coagulation. This method enabled both the reduction of the mean size of Au and Ag nanoparticles down to 4-8 nm and the minimization of the particle size dispersion down to 5 nm. However, the fabrication of monodispersed gold nanoparticles in well-controlled, biologically friendly environment and appropriate termination of the gold surface is still under question.

In our recent works[17-19], we studied physical and chemical factors of the particle size control by using quite different radiation parameters and different reducing agents. First, we ablated targets by a femtosecond laser with the anticipation to reduce the size and dispersion of nanoparticles due to the absence of target heating effects[50] and much higher threshold of the liquid breakdown compared to longer pulses[51]. Second, we used biologically compatible reducing agents, which enabled to avoid the chemical termination of the gold surface. Basically, we used neutrally charged cyclodextrins (CD) (α-CD, β-CD and γ-CD), torus-like macrocycles built up from glucose pyranose units, which are linked by α-1-4-linkages[52].

The experiments were carried out with a Ti/Sapphire laser (Hurricane, Spectra Physics Lasers, Mountain View, CA), which provided 110 fs full width at half maximum (FWHM) pulses (wavelength 800 nm, maximum energy 1 mJ/pulse, repetition rate of 1 kHz). The radiation was focused by an objective with the focal distance of 7.5 cm onto a gold target, which was placed on the bottom of a 3-mL glass vessel filled with different aqueous solutions. The thickness of the liquid layer above the rod was about 12 mm. The vessel was placed on a horizontal platform, which executed repetitive circular motions at a constant speed of 0.5 mm/s to form circle- like ablated region on the target surface. A gold rod with the diameter of 6 mm and the height of 6 mm was used as a target in the experiments. The ablation experiments were carried out in pure deionized water and in aqueous solutions of α-cyclodextrin, β-CD, and γ-CD, used without further purification. All solutions were prepared from high-purity deionized water. CD solutions were prepared as stock

solutions in appropriate buffers immediately prior to their use. The concentration of cyclodextrins was varied in different experiments: 0.01 M, 0.001 M and 0.0001 M.

First, we studied possibilities for the particle size control by purely chemical mechanisms. Basically, we carried out the ablation experiments under different concentrations of CDs at a fixed laser fluence of 600 J/cm^2. Fig. 7 shows typical TEM micrograph images of laser-produced nanoparticles and corresponding size distributions, obtained by examining sizes of at least 1000 nanoparticles. One can see that in pure deionized water (Fig. 7a), the ablation process led to particle sizes of 40-70 nm, however, a rather broad size distribution ranging from 25 nm to 140 nm was noted. This distribution corresponded to purple-red color of the solution with some yellow tint. However, the presence of cyclodextrins in the solution resulted in a dramatic decrease of the size of produced particles and their size dispersion, as one can see from Fig. 7b. The mean nanoparticle size and dispersion depended both on the CD concentration and on its type with the smallest size and narrowest dispersion for β-CD, followed by γ-CD and α-CD (Fig. 7 c, d). Ablation in 10 mM β-CD produced particles with the mean size of 2.1-2.3 nm and the dispersion of less than 1 nm FWHM (Fig. 7c, d). This distribution corresponded to a deep red color of the solution. For a comparison, the laser ablation in the presence of 100 mM SDS led to much larger 4.6-8 nm particles with the dispersion of 5 nm FWHM[43,45]. Notice that chemical analysis performed in this study confirmed that not even traces of glucose, a major degradable products of CDs was present in the solution. In view of the very mild condition in laser ablation, it could be reasoned that CD molecules remained intact during the course of experiment.
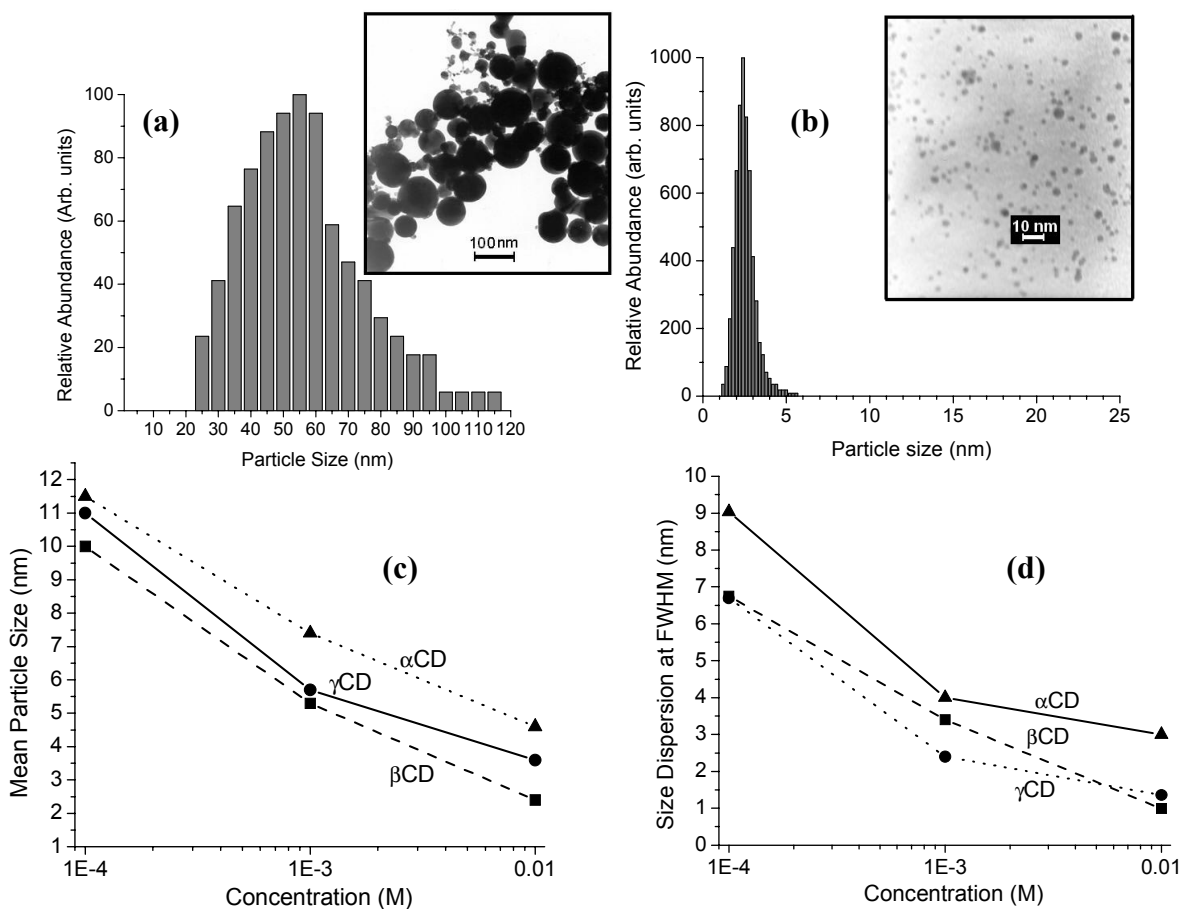

Fig. 7 TEM micrograph images and corresponding size distributions of gold particles prepared by the femtosecond laser ablation in deionized water (a) and in 0.01 M β-CD (b). Effect of the CD concentration on the resulting average particle size (c) and the size dispersion at FWHM (d)

The produced particles exhibited the plasmon-related peak in the extinction spectra, as shown in Fig. 8. For nanoparticles prepared in CDs, this peak was around 520-530 nm that was consistent with the presence of small 3-30 nm particles in the solution[37]. However, for nanoparticles prepared in water the peak suffered a broadening and a red shift to 540-550 nm, suggesting a certain "dephasing" of signals from individual plasmons due to an increase of particle size and dispersion. In pure water, the absorbance measured at 520 nm retained only 7% of its original value after 5 days of aging in ambient conditions. Several precipitates were observed in the storage glass vial and the solution became dark blue, which confirmed that the nanoparticles continued to grow and/or aggregate with time in the solution. This behavior was due largely to the rapid increase in the attractive van der Waals force between nanoparticles as a function of their size. In contrast, gold colloids prepared in the presence of CDs were very stable. In particular, nanoclusters β-CD remained well dispersed in 10 mM β-CD for over one year with minimal loss of absorption intensity (5-7 %). This was very encouraging since all of the experiments were performed without any precaution taken, such as oxygen-free condition or under protective agents except for CDs. Studies of the reduction mechanism by CDs are now in progress[53].
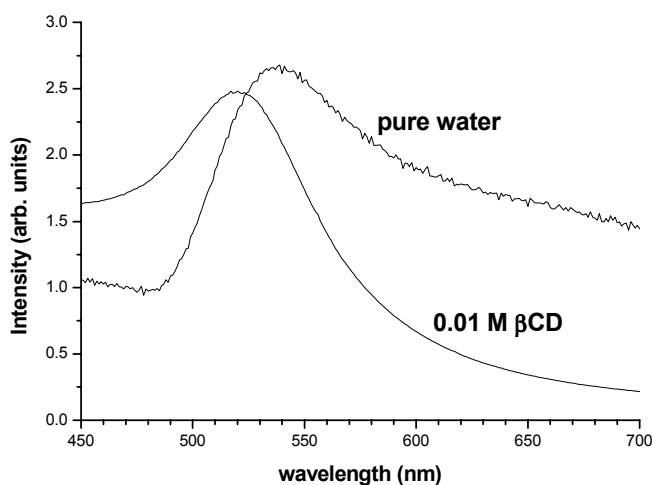

Fig. 8 Typical optical absorption spectra of gold nanoparticles prepared in pure deionized water and 10 mM of β-CD

Secondly, we studied possibilities for the size control by using physical mechanisms. In this case, the experiments were carried out in pure deionized water without any chemical reducing agent. The main variable parameter was the laser fluence, whose value was controlled by changing the laser energy. Fig. 9 shows typical TEM micrographs of particles produced at different laser fluences. One can see that a fluence decrease led to a drastic particle size reduction. Indeed, the mean particle size dropped from 120 to 4 nm as F decreased from 1000 J/cm^2 to 60 J/cm^2. Notice that with nanosecond laser ablation only a weak nanoparticle size control was possible by changing physical parameters[43,48]. In is interesting to note that for lowest ($F < 100$ J/cm^2) and highest ($F > 400$ J/cm^2) fluences the size distributions could easily be extrapolated by Gaussian functions. However, for intermediate fluences between 100 J/cm^2 and 400 J/cm^2 the single-peak Gaussian extrapolation was not adequate. An example of such distribution is shown in Fig. 9b, in which most particles are relatively small with the mean size around 5-10 nm, but a significant number of very large 10-80 nm particles are still present in the solution and the resulting dispersion is rather high. It is known that distributions like these are well described by two Gaussian functions with separated maxima, suggesting that two different mechanisms are involved in the nanoparticle production.

To better understand possible reasons of the particle distribution variations, we performed a SEM study of craters on the gold surface produced by the femtosecond laser ablation in water. As shown in Fig. 10, the craters formed under low and high fluences were quite different. For low fluences Fig. 10a, the walls of craters were smooth without any indication on the contribution of heating effects. In contrast, the craters prepared at high fluences F > 100 J/cm^2 (Fig. 10b) were broader and had irregular profiles, while their walls and bottoms contained traces of molten material. In addition, the later craters were surrounded by a significant heat-affected zone.

Thus, properties of nanoparticles prepared by the femtosecond laser ablation were quite different compared to the nanosecond ablation case[43-47]. Indeed, the femtosecond ablation made possible a reduction of the particle size down to 4-5 nm without any chemical reducer and the simultaneous production of two size distributions at high laser fluences, while the nanosecond ablation led to much larger particles. We believe that such a difference is related to different conditions of plasma production. As known from the literature (see, e.g., 51), the laser ablation in liquids is often accompanied by a breakdown phenomenon, which leads to a significant absorption of radiation energy in the breakdown plasma near the target. Then, the plasma energy release is accompanied by the formation of a cavitation bubble in the liquid, which collapses 150-200 μs after the laser pulse. The bubble collapse generally gives rise to the interaction of a cavitation wave with the target and a more intense secondary ablation of material from the target as a result of this interaction. Since the breakdown threshold is 10-fold lower for the nanosecond radiation compared to the femtosecond one, it is difficult to avoid the breakdown phenomenon in the case of the nanosecond radiation. Therefore, the nanosecond case is characterized by an efficient formation of the bubble, which then leads to the formation of relatively large particles. In our opinion, similar situation takes place under high fluences of the femtosecond radiation, when large particles are formed due to the cavitation-related ablation (Fig. 9a). However, femtosecond laser ablation at low fluences enables one to avoid the breakdown phenomenon and achieve much better radiation transfer to the target surface. This causes an efficient radiation-related ablation of the material and the appearance of the second "narrow" distribution of the produced particles with the mean size of less that 10 nm (Fig. 9 b,c).
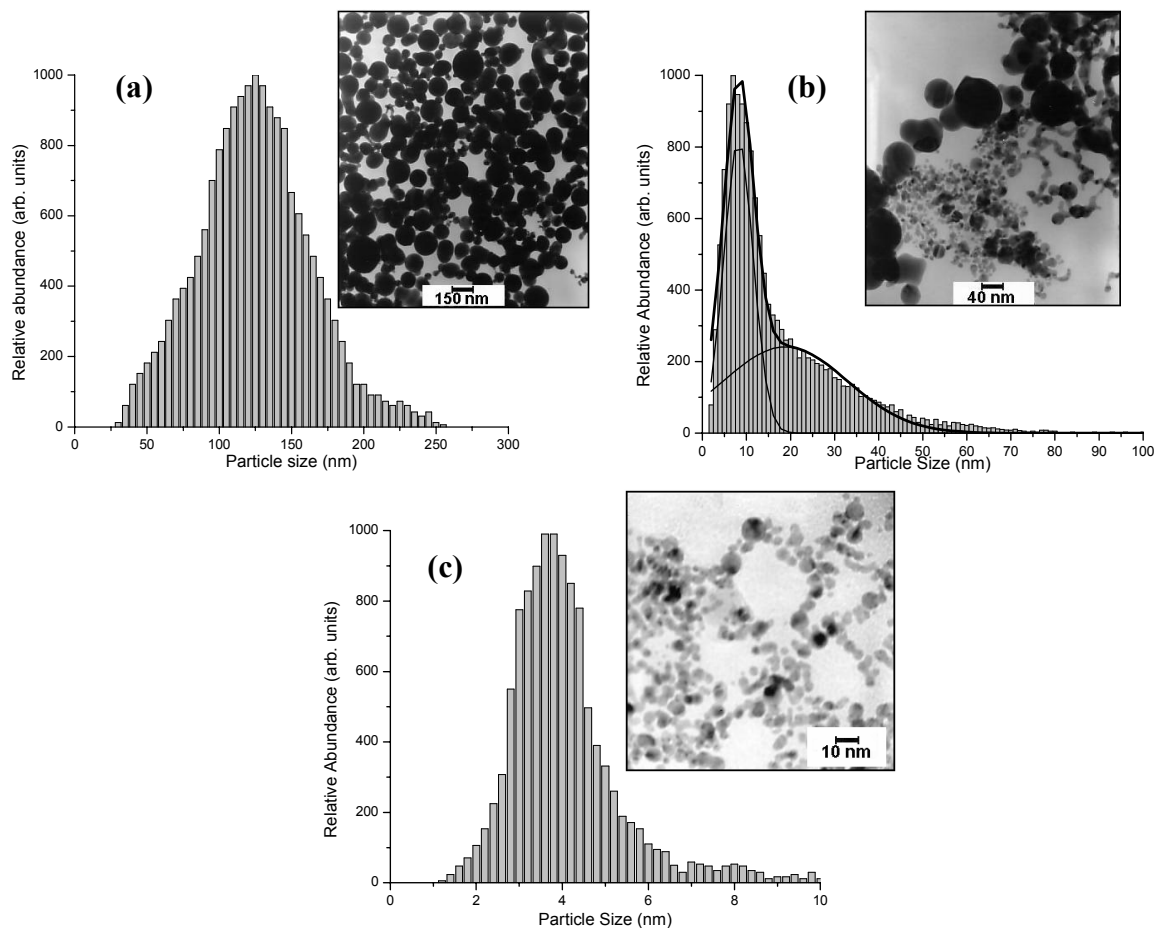

Fig. 9 TEM micrograph images and corresponding size distributions of gold nanoparticles prepared by the femtosecond laser ablation in deionized water at different fluences; (a) 1000 J/cm^2 (b) 160 J/cm^2 and (c) 60 J/cm^2.
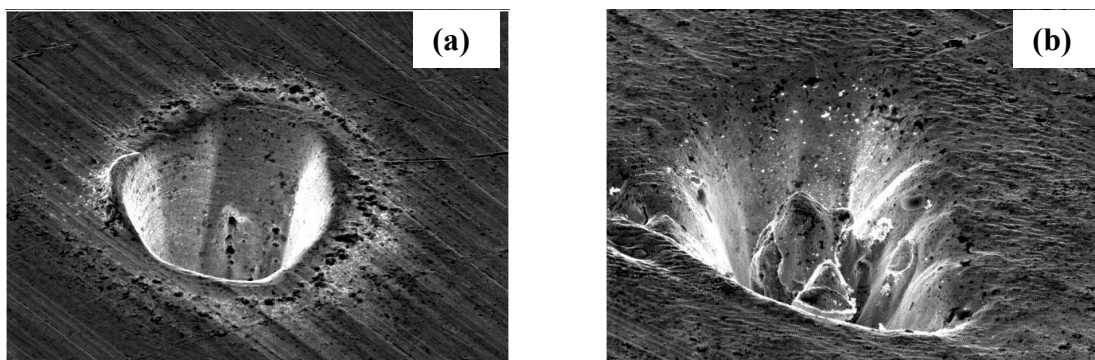
Fig. 10 Typical craters on the gold target in water after 5000 laser pulses at $F = 60$ J/cm^2 (a) and $F = 1000$ J/cm^2 (b).

Thus, our studies have clearly showen that the femtosecond laser radiation gives better opportunities for the nanoparticle fabrication control in the liquid ambience.

CONCLUSIONS

Different laser-assisted methodologies for nanofabrication have been developed and applied for the fabrication of nanoparticles/nanostructures in the gaseous and liquid environment. Synthesized materials exhibit unique properties and characteristics, which make them very important for biosensing and photonics applications.

ACKNOWLEDGEMENTS

REFERENCES

1. J. F. Ready, D. F. Farson, Eds.; *LIA Handbook of Laser Materials Processing*, Springer-Verlag and Heidelberg GmbH & Co., Berlin, 2001.
2. L. A. Chiu, A. A. Seraphin, and K. D. Kolenbrander, *J. Electron. Matter* **23** pp. 347-353, 1994.
3. I. A. Movtchan, W. Marine, R. W. Dreyfus, U. C. Lee, M. Sentis, and M. Autric, "Luminescence from a Si-SiO$_2$ nanocluster-like structure prepared by laser ablation", *Appl. Surf. Sci.*, **96-98** pp. 251-258, 1996.
4. D. B. Geohegan, A. A. Puretzky, G. Duscher, and S.J.Pennycook, *Appl. Phys Lett.*, **72** pp. 2987-2989, 1998.
5. Yu.P. Raizer *Laser-Induced Discharge Phenomena*, Consultants Bureau, New York, 1977.
6. A.V.Kabashin, M.Meunier, "Air optical breakdown on silicon as a method of fabrication of photoluminescent Si-based nanostructures", *Proc. SPIE*, **4636**, pp. 59-66, 2002.
7. A.V.Kabashin, M.Meunier, "Fabrication of photoluminescent Si-based layers by air optical breakdown near the silicon surface", *Appl. Surf. Sci.*, **186**, pp. 576-582, 2002.
8. A.V. Kabashin, M. Meunier, "Visible photoluminescence from nanostructured Si-based layers produced by air optical breakdown on silicon", *Appl. Phys. Lett*, **82**, pp. 1619-1621, 2003.
9. A.V. Kabashin, M. Meunier, "Laser-induced treatment of silicon in air and formation of Si/SiO$_x$ photoluminescent nanostructured layers", *Mat. Sci Eng. B*, **101**, pp. 60-64, 2003.
10. A. V. Kabashin, V-G. Pilon Marien, D.-Q. Yang, F. Magny, and M. Meunier, "Porous nanostructured layers on germanium produced by laser optical breakdown processing", *Proc. SPIE*, **4977**, 632-638, 2003.

11. D.-Q. Yang, A.V. Kabashin, V-G. Pilon Marien, E. Sacher, M. Meunier, "Optical Breakdown processing: influence of ambient gas on properties of formed nanostructured Si-based layers", *J. Appl. Phys*., in press, 2004.

12. A.V. Kabashin, M. Charbonneau-Lefort, M. Meunier et R. Leonelli, "Production of PL Si-based nanostructures by laser ablation: effects of ablation and post-deposition conditions", *Proc. SPIE*, **3933**, pp.192-199, 2000.

13. A.V. Kabashin, M. Charbonneau-Lefort, M. Meunier et R. Leonelli, "Effects of deposition and post-fabrication conditions on PL properties of nanostructured Si/SiOx films prepared by laser ablation", *Appl. Surf. Sci*., **168** pp. 328-331, 2000.

14. A. V. Kabashin, M. Meunier, R. Leonelli, "PL characterization of Si-based nanostructured films produced by pulsed laser ablation in an inert residual gas", *J. Vac. Sci. Tech. B*, **19** pp. 2217-2225, 2001.

15. A.V. Kabashin, J.-P. Sylvestre, S. Patskovsky, M. Meunier, "Variable porous structure of laser-ablated silicon nanocluster films and its influence on photoluminescence properties", *Proc. SPIE*, **4636**, pp. 38-47, 2002.

16. A.V. Kabashin, J-P. Sylvestre, S. Patskovsky, M. Meunier, "Correlation between PL properties and morphology of laser-ablated Si/SiO$_x$ nanostructured films", *J. Appl. Phys*., **91** pp. 3248-3254, 2002.

17. A.V. Kabashin, M. Meunier, C. Kingston, J. H. T. Luong, "Fabrication and Characterization of Gold Nanoparticles by Femtosecond Laser Ablation in Aqueous Solution of Cyclodextrins", *J. Phys. Chem B*, **107**, pp. 4527-4531, 2003

18. A.V. Kabashin, M. Meunier, J. H. Luong, "Femtosecond laser ablation of gold in aqueous biocompatible solutions to produce colloidal gold nanoparticles", *Proc. SPIE*, **4977**, pp. 609-614, 2003.

19. A.V. Kabashin, M. Meunier, "Synthesis of colloidal nanoparticles during femtosecond laser ablation of gold in water", *J. Appl. Phys*., 94, pp. 7941-7943, 2003

20. L. T. Canham, "Silicon quantum wire array fabrication by electrochemical and chemical dissolution of wafers", *Appl. Phys. Lett*., **57**, pp. 1046-1048, 1990.

21. S. M. Prokes, "Light emission in thermally oxidized porous silicon: Evidence for oxide-related luminescence", *Appl. Phys. Lett.*, 62, pp. 3244-3252, 1993.

22. H. Takagi, H. Ogawa, Y. Yamazaki, A. Ishizaki, and T. Nakagiri, "Quantum size effects on photoluminescence in ultrafine Si particles", *Appl. Phys. Lett*., **56**, pp. 2379-2380, 1990.

23. Y. Kanemitsu, T. Ogawa, K. Shiraishi, and K. Takeda, Visible photoluminescence from oxidized Si nanometer-sized spheres: exciton confinement on a spherical shell", *Phys Rev. B*, **48**, pp. 4883-4886, 1993.

24. M. Ehbrecht, B. Kohn, F. Huisken, M.A. Laguna, and V. Paillard, " Photoluminescence and resonant Raman spectra of silicon films produced by size-selected cluster beam deposition", *Phys. Rev., B,* **56** pp. 6958-6963, 1997.

25. K.S.Min, K.V. Shcheglov, C.M. Yang, H.A.Awater, M.L.Brongersma, and A.Polman, "Defect-related versus excitonic visible light emission from ion beam synthesized Si nanocrystals in SiO$_2$", *Appl. Phys. Lett*., **69** pp. 2033-2038, 1996.

26. E. Werwa, A. A. Seraphin, L. A. Chiu, Chuxin Zhou, and K. D. Kolenbrander, **"**Synthesis and processing of silicon nanocrystallites using a pulsed laser ablation supersonic expansion method**" ,** *Appl. Phys. Lett*., **64** pp. 1821-1823, 1994.

27. I. A. Movtchan, R. W. Dreyfus, W. Marine, M. Sentis, M. Autric, G. Le Lay and N. Merk, "Luminescence from a Si-SiO$_x$ nanocluster-like structure prepared by laser ablation", *Thin Solid Films*, **255**, pp. 286-289, 1995.

28. Y. Yamada, T. Orii, I. Umezu, Sh. Takeyama, and T. Yoshida, "Optical properties of silicon nanocrystallites prepared by excimer laser ablation in inert gas", *Jpn. J. Appl. Phys., Part 1*, **35**, pp.1361-1365, 1996.

29. T. Makimura, Y. Kunii, and K. Murakami, "Light emission from nanometer-sized silicon particles fabricated by the laser ablation method", ", *Jpn. J. Appl. Phys., Part 1*, **35**, pp.4780-4784, 1996.

30. L. Patrone, D. Nelson, V. I. Safarov, M. Sentis, W. Marine, S. Giorgio, "Photoluminescence of silicon nanoclusters with reduced size dispersion produced by laser ablation ", *J. Appl. Phys*., **87,** pp. 3829-3837, 2000.

31. L. T. Parratt, "Surface studies of solids by total reflection of x-rays", *Phys. Rev.,* **95**, pp. 359-369, 1954.

32. R.E Hummel, S-S. Chang**, "**Novel technique for preparing porous silicon", *Appl. Phys. Lett.,* **61**, pp. 1965-1967, 1992.

33. E.F. Steigmeier, H. Auderset, B. Delley, and R. Morf, "Visible light emission from Si materials*", J. Luminescence,* **57,** pp. 9-12, 1993.

34. R.E. Hummel, A. Morrone, M. Ludwig, and S.-S. Chang, "On the origin of photoluminescence in spark-eroded (porous) silicon", *Appl. Phys. Lett*., **63,** pp. 2771-2773, 1993.

35. M.H. Ludwig, A. Augustin, and R.E. Hummel, "Colour-switching effect of photoluminescent silicon after spark-processing in oxygen", *Semicond. Sci. Technol.*, **12,** pp. 981-986, 1997.

36. S. Munekuni, T. Yamanaka, Y. Shimogaichi, K. Nagasawa, and Y. Hama, "Various types of nonbridging oxygen hole center in high-purity silica glass", *J. Appl. Phys*. **68,** pp. 1212-1221, 1990.

37. M. Kerker, The *scattering of light and other electromagnetic radiation,* Academic Press, New York, 1969.

38. U. Kreibig, M. Vollmer, *Optical Properties of Metal Clusters*, Springer-Verlag: Berlin, 1996.

39. M. A. Hyatt, Ed. *Colloidal Gold: Principles, Methods, and Applications*, Academic Press: New York, **3**, 1989.

40. A. Fojtik, A. Henglein, *Ber. Bunsen-Ges. Phys. Chem*, **97**, pp. 252-260, 1993.

41. M. S. Sibbald, G. Chumanov, T. M. Cotton, *J. Phys. Chem.*, **100**, 4672, 1996.

42. M. S. Yeh, Y. S. Yang, Y. P. Lee, H. F. Lee, Y. H. Yeh, S. S. Yeh, *J. Phys. Chem.*, **103**, pp. 6851-6859, 1999.

43. F. Mafune, J-Y. Kohno, Y. Takeda, T. Kondow, H. Sawabe, *J. Phys. Chem.*, *B*, **104**, 9111, 2000.

44. F. Mafune, J-Y. Kohno, Y. Takeda, T. Kondow, H. Sawabe. *J. Phys. Chem*., **104**, 8333. 2000.

45. F. Mafune, J-Y. Kohno, Y. Takeda, T. Kondow, H. Sawabe, "Formation of gold nanoparticles by laser ablation in aqueous solution of surfactant", *J. Phys. Chem. B.,* **105**, pp. 5144-5120, 2001.

46. Y.-H. Chen, and C.-S. Yeh, *Colloids & Surfaces*, **197**, pp. 133-138, 2002.

47. S. I. Dolgaev, A. V. Simakin, V. V. Voronov, G. A. Shafeev, and F. Bozon-Verduraz, "Nanoparticles produced by laser ablation of solids in liquid environment", *Appl. Surf. Sci.,* **186,** pp. 546-551, 2002.

48. T. Tsuji, K. Iryo, N. Watanabe, and M. Tsuji, *Appl. Surf. Sci.* **202,** pp. 80-85, 2002.

49. T. Tsuji, T. Kakita, and M. Tsuji, "Preparation of nano-size particles of silver with fs laser ablation in water", *Appl. Surf. Sci.* **206,** pp. 314-320, 2003.

50. J. F. Ready, D. F. Farson, Eds.; *LIA Handbook of Laser Materials Processing*, Springer-Verlag and Heidelberg GmbH & Co., Berlin, 2001; pp. 499-508.

51. A. Vogel et. al., "Energy balance of optical breakdown in water at nanosecond to femtosecond time scale", *Appl. Phys. B*, **68**, pp. 271-280, 1999.

52. J. Szejtli, In *Comprehensive Supramolecular Chemistry*, Atwood, J.L., Davies, J.E.D., Macnicol, D.D., Vogtle, F., Eds.; Pergamon-Elsevier, New York, 1996; Vol. 3; pp. 5-40.

53. J.-P. Sylvestre, A. V. Kabashin, E. Sacher, M. Meunier and J. H. T. Luong, "Nanoparticle size reduction during laser ablation in aqueous solutions of cyclodextrins", *Proc. SPIE*, **5339**, in press, 2004.